Program Digest, 2019 IEEE International Ultrasonics Symposium (IUS)
Glasgow, Scotland, October 6-9, 2019

A High Velocity and Wideband SAW on a Thin $LiNbO_3$ Plate Bonded on a Si Substrate in the SHF Range

Tetsuya Kimura, Masashi Omura, Yutaka Kishimoto, Haruki Kyoya, Masakazu Mimura, and Hiromu Okunaga
Murata Manufacturing Co., Ltd., Kyoto, Japan

Ken-ya Hashimoto
Graduate School of Enginerring, Chiba University, Chiba, Japan

***Abstract*— Although it was considered to be impractical to apply surface acoustic wave (SAW) filters in the super high frequency (SHF) range, a technology recently revealed that use of a thin piezoelectric crystal plate may recreate an impression of the past. This paper describes acoustic wave devices comprising the thin piezoelectric crystal plate, interdigital transducers placed on the plate, and an acoustic mirror bonded on a silicon substrate. First, it is theoretically and experimentally shown how the acoustic energy can be confined in the top surface even though longitudinal leaky SAW (LLSAW) is utilized. Then it is shown how the proposed structure is promising for the SHF range filters in mobile terminals upcoming next generation wireless access technology through comparing with the incredible high performance SAW (I.H.P. SAW) and a high velocity A_1 Lamb wave resonator.**

***Keywords*— bulk acoustic wave (BAW), filter, Lamb wave, resonator, surface acoustic wave (SAW).**

I. INTRODUCTION

Data traffic of wireless communication system has been increasing [1], and a sophisticated new generation of mobile communication system has introduced to address the increase of traffic demands roughly every ten years. Higher and wider frequencies have been assigned for the system as generations go by [2]. Therefore, it is natural that surface acoustic wave (SAW) and bulk acoustic wave (BAW) devices in handsets are strongly requested to support such higher and wider frequency spectrum bands.

In reference to the SAW filters, a driving frequency f_0 of the SAW filter is given by

$$f_0 \approx \frac{V}{\lambda} \tag{1}$$

where V is a phase velocity and λ is a wavelength of the SAW. Technique of shrinking interdigital transducers (IDT) has been conventionally applied for realizing desired high frequencies to the SAW devices. However, producing much narrower electrodes and gaps of the IDT requires more sophisticated lithography systems such as an ArF excimer laser (wavelength: 193 nm) that overwhelms an i-line (wavelength: 365 nm) and a KrF excimer laser (wavelength: 248 nm) that are currently used in the SAW mass production. Introduction of the new equipment may cause increase of fabrication costs.

Equation (1) suggests another approach to use of high velocity SAW modes for obtaining a high f_0. A lot of high velocity SAW modes have been reported. For example, uses of the second mode called the Sezawa mode [3] with multi layered structures comprising high velocity materials such as sapphire, diamond and 6H-SiC and piezoelectric thin films such as ZnO and AlN [4-10].

High frequency filters are realizable owing to their large phase velocities, however, their electromechanical coupling factor k^2 are smaller than those of leaky SAWs on 36-48°Y cut $LiTaO_3$ (LT) substrates and temperature compensated Rayleigh SAWs on $LiNbO_3$ (LN) substrates; they are called 42LT and TC-SAW, respectively, that have been widely used for mobile terminals.

Another suggestion is use of longitudinal leaky SAW (LLSAW) modes travelling on LT, LN and $Li_2B_4O_7$ substrates and having larger phase velocities than those of share horizontal (SH) and share vertical (SV) modes on the substrates [11-15]. Among this group, the LLSAW travelling on an X cut LN substrate provides larger k^2 than those of the 42LT and TC-SAW. However, previously reported propagation losses of the LLSAW are much larger than those of the conventional SAWs. To make matters worse, their temperature coefficient of frequency (TCF) are also relatively worse compared to the conventional ones. Many studies have been attempted to improve characteristics of the LLSAW devices, nevertheless, achieved performances were limited, accordingly, the LLSAW modes have not been used for SAW devices in mobile handsets.

Recently, multilayered structure using a single crystal piezoelectric thin plate has been paid attention as a breakthrough technology in the present SAW devices. Takai *et al*. demonstrated that extremely low-loss and low TCF SAW devices, they named it incredible high performance SAW (I.H.P. SAW), at 1.9 and 2.45 GHz by using a rotated Y cut LT thin crystal plate bonded on a silicon substrate [16,17]. After that, similar concepts have been also emerged by several authors [18-24].

The technology called I.H.P. SAW is capable to solve the problems of insertion losses and TCFs of the SAW devices which have been thought to be intrinsic disadvantage of the conventional SAW devices against BAW devices. However, even though the promising performances, since the use of the rotated Y cut LT thin crystal plates and their SH modes restricts their k^2 and V, it may be difficult to meet filter requirements for higher frequencies with wider bandwidths in the upcoming next generation of mobile communication systems.

The authors reported a composite substrate comprising an X cut LN thin crystal plate and an acoustic mirror on a handle substrate to improve characteristics of the LLSAW that is known as relatively large k^2 and V but large propagation loss and TCF [25].

This paper reviews the suggested LLSAW device structure. First, it is shown theoretically that how the acoustic wave energy is well confined in the vicinity of the top surface. Next, it is shown that the effect of the acoustic mirror by observation of the LLSAW vibration with a laser probe system. After that, the performances of fabricated 3.5 and 5 GHz 1-port LLSAW resonators on the structure are described. Finally, they are compared and discussed with the I.H.P. SAW and an A_1 mode Lamb wave devices which both use piezoelectric thin crystal plates.

II. Theoretical Results and Discussion

At the beginning, a multilayered structure substrate is discussed. It consists of IDT, a single crystal thin piezoelectric plate, energy confinement layer(s) and a handle substrate as shown in Fig. 1. The structure enables good acoustic energy confinement in the vicinity of the top surface, thus acoustic waves in the thin piezoelectric plate behave like plate modes. In this paper, we classify these acoustic waves traveling on the multilayered substrates as the SAW group, because overall structure of the devices is not a free standing thin plate but the composite substrates whose thickness is much greater than the wavelength of the travelling acoustic waves in the thin crystal piezoelectric plate.

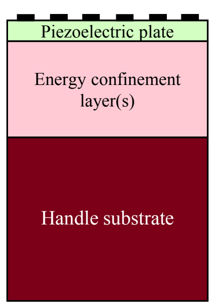

Fig. 1. Conceptual device structure discussed in this paper.

A. Application of I.H.P. SAW technique to the LLSAW

In this part, application of the I.H.P. SAW technique to the LLSAW is discussed. Fig. 2 shows a variation of the I.H.P. SAW device structure composed of the IDT, the thin piezoelectric plate, an SiO_2 layer as a temperature compensation portion bonded on a silicon substrate which works as a high velocity handle substrate. As described in [16], when a rotated Y cut LT is used for the piezoelectric plate and the silicon is used for the high velocity handle substrate, the structure makes it possible to trap the acoustic energy in the vicinity of the layered substrate, because the velocities of the SH type bulk acoustic waves traveling in the silicon substrate is larger than that of an SH wave propagating in the thin LT plate. In addition, when the SiO_2 film is utilized as the optional layer, its TCF can be improved.

Let us consider the same configuration as shown in Fig. 2, where an X cut 40°Y LN is applied to the piezoelectric plate instead of the rotated Y cut LT. In this case, the LLSAW can be excited by the IDT. Several materials are examined as the high velocity handle substrates.

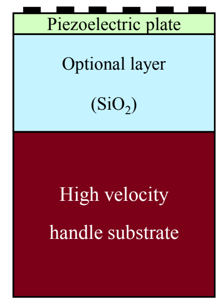

Fig. 2. A variation of the I.H.P. SAW device structure.

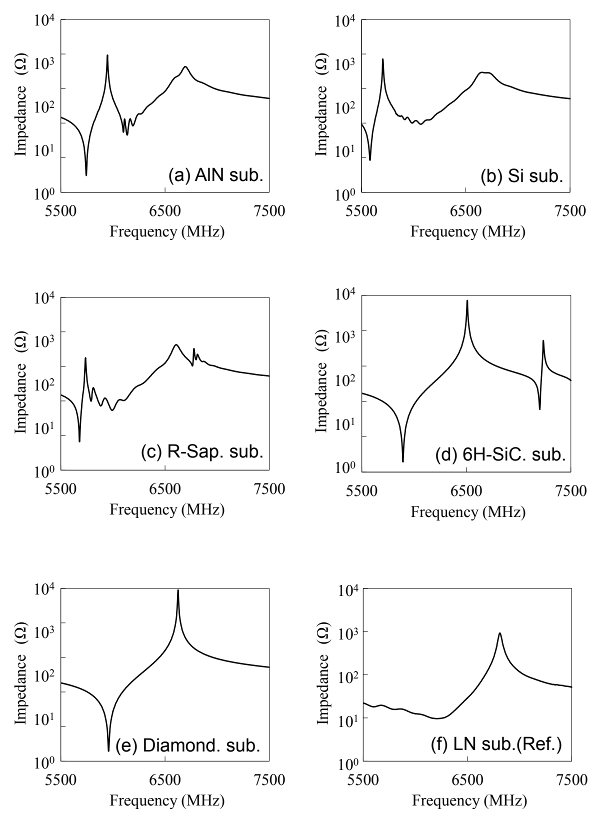

Fig. 3. Simulated impedance curves of 1-port LLSAW resonators using the I.H.P. SAW device structure shown in Fig. 2.
(a) AlN, (b) Si(100), (c) R-plane sapphire, (d) 6H-SiC and (e) diamond substrates are chosen for the high velocity handle substrates. (f) represents an impedance curve of the traditional LLSAW propagating on the X cut 40°Y LN substrate as a reference.

TABLE I. VELOCITIES OF THE MATERIALS FOR A HIGH VELOCITY HANDLE SUBSTRATE.

		(a) AlN (0°,0°,0°)	(b) Si(100) (0°,0°,45°)	(c) R-plane Sapphire (0°,122.23°,0°)	(d) 6H-SiC (0°,0°,0°)	(e) Diamond (0°,0°,0°)
Longitudinal wave velocity	V_L (m/s)	10,287	8,433	11,175	12,491	17,541
Faster transverse wave velocity	V_{FT} (m/s)	6,016	5,845	6,766	7,125	12,810
Slower transverse wave velocity	V_{ST} (m/s)	6,016	5,845	5,744	7,125	12,810

Fig. 3 shows simulated impedance curves of 1-port LLSAW resonators when thicknesses of the X cut 40°Y LN and SiO_2 layers are set at 0.2λ and 0.15λ, respectively, and either (a) AlN, (b) Si(100), (c) R-plane sapphire, (d) 6H-SiC or (e) diamond is chosen for the high velocity handle substrate. In addition, the characteristic of the traditional LLSAW on the X cut 40°Y LN substrate case (f) is also shown in Fig. 3 as a reference. In this simulation, λ is 1 μm, and material of the IDT is Al and the thickness is 0.05λ.

It is clearly seen that the characteristics of the resonators deteriorate when the substrate (a), (b) or (c) is used. On the other hands, characteristics are satisfactory when the substrate (d) or (e) is employed. This is because the transverse waves velocities for (a), (b) and (c) are not larger than the LLSAW in the LN plate as shown in Table I. Note that the longitudinal wave velocities for (a) to (e) are much larger than that of the LLSAW in the LN plate.

Although it is theoretically possible to obtain favorable characteristics when the 6H-SiC or diamond is employed, it seems to be hard to apply these materials to SAW mass production owing to their size, price and quality at this time.

B. Application of an acoustic mirror to the LLSAW

In this part, more practical device structure is discussed for the LLSAW instead of the introduction of the 6H-SiC and diamond. The authors proposed another LLSAW device structure comprising the IDT, the thin piezoelectric plate, an acoustic mirror bonded on a handle substrate as depicted in Fig. 4 [25-27]. The acoustic mirror is composed of low-acoustic-impedance (LAI) and high-acoustic impedance (HAI) layers stacked alternately beneath the piezoelectric plate. The Bragg reflection enables good acoustic energy confinement in the vicinity of the surface as that used in solidly mounted resonator type BAW devices [28-33].

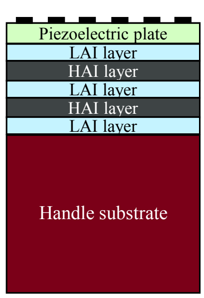

Fig. 4. Another variation of the LLSAW device structure comprising IDT, the thin piezoelectric plate, an acoustic mirror bonded on a handle substrate.

It should be noted that the acoustic mirror may work under proper design even when the velocities of bulk acoustic waves in the LAI/ HAI materials and the handle substrate are slower than those in the piezoelectric layer.

Next, the acoustic mirror performance is calculated by matrix techniques [34]. In this paper, five layers in total multilayered acoustic mirror comprising the LAI and HAI materials is assumed as illustrated in Fig. 5. Here, SiO_2 is always assigned to the LAI layers because the SiO_2 works effectively as not only the LAI but also temperature compensation. Then, AlN, Ta_2O_5, HfO_2, Ta, Pt, W and Ir are examined as the HAI materials.

Here, β_x in Fig. 5 is the wavenumber of the SAW propagating on the surface, which is expressed as

$$\beta_x = \frac{2\pi}{\lambda_x} \quad (2)$$

where λ_x is the SAW wavelength determined by the IDT periodicity, and λ_x is set to 1.7 μm in this case. Each thickness of the layer in the acoustic mirror equals to a quarter-wavelength thickness ($\lambda_z/4$) at 3.5 GHz.

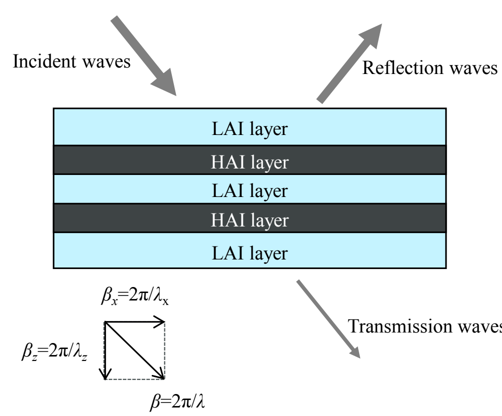

Fig. 5. Assumed five layers in total multilayered acoustic mirror for calculation of the performance.
LAI layer: SiO_2 (always applied)
HAI layer: AlN, Ta_2O_5, HfO_2, Ta, Pt, W and Ir.

Fig. 6 shows the calculation results of the transmission coefficient of the acoustic mirror. The transmission wave energy is normalized by the incident wave energy. Legends in Fig. 6 line from top to down in order of less acoustic impedance of the HAI materials. It is clearly seen that the larger acoustic impedance of the HAI material has, the smaller transmission coefficient and the wider stopband width.

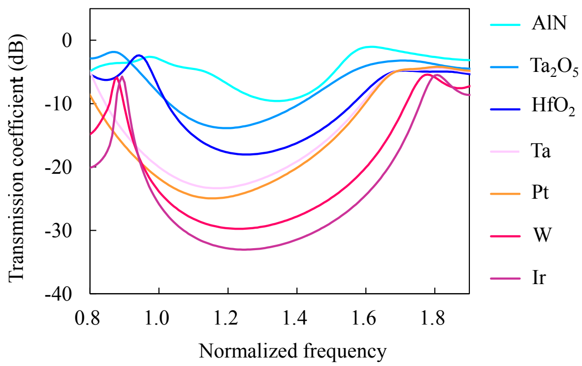

Fig. 6. Calculation results of the transmission coefficient of the acoustic mirror.

Next, characteristics of 1-port LLSAW resonators using several configurations of acoustic mirror are calculated by the finite element method (FEM). Detailed configurations of the resonator structures for the simulation are shown in Table II. The calculated impedance curves of the resonators are compared in Fig. 7. According to the simulation results, much wider fractional bandwidth is obtainable when much larger acoustic impedance material is used for the HAI layer. There is, however, negligible difference among the performances using Ta, Pt, W and Ir for the HAI material.

Fig. 8 shows simulated cross-sectional field distribution of the structure using several configurations of the acoustic mirrors. It is seen how good energy confinement in the thin LN plate is realizable when Ta, Pt, W and Ir are used for the HAI layers. On the contrary, when AlN is applied to the HAI layers, it is seen the relatively poor energy confinement in the LN thin plate due to non-negligible BAW leakage to the silicon substrate. Thus, the good energy confinement in the LN plate may result in the wider fractional bandwidth of 1-port LLSAW resonators when larger acoustic impedance materials are used for the HAI layers as depicted in Fig. 7.

TABLE II. 1-PORT LLSAW STRUCTURAL PARAMETERS FOR CALCULATION.

IDT	Al(125 nm) Wave length(λ_x) : 1.7 μm
Piezoelectric plate	(90°,90°,40°) $LiNbO_3$ Thickness : 340 nm
Acoustic mirror	Five layers acoustic mirror composed of SiO_2 and each HAI material HAI : AlN, Ta_2O_5, HfO_2, Ta, Pt, W, Ir Each layer thickness corresponds to those of $\lambda_z/4$ at 3.5 GHz
Handle substrate	Silicon

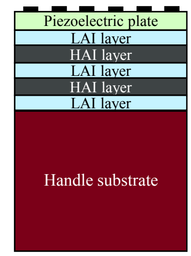

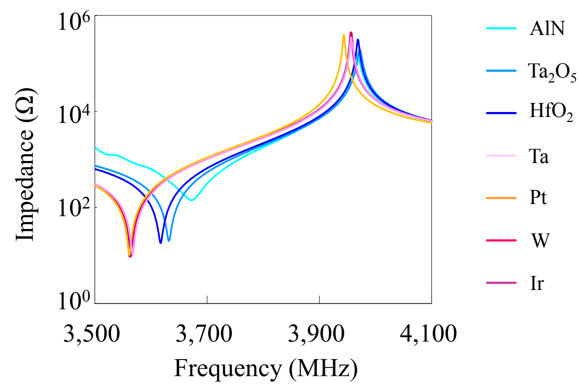

Fig. 7. Comparison of the calculated impedance curves among several configurations of the acoustic mirror. The legends show the HAI materials.

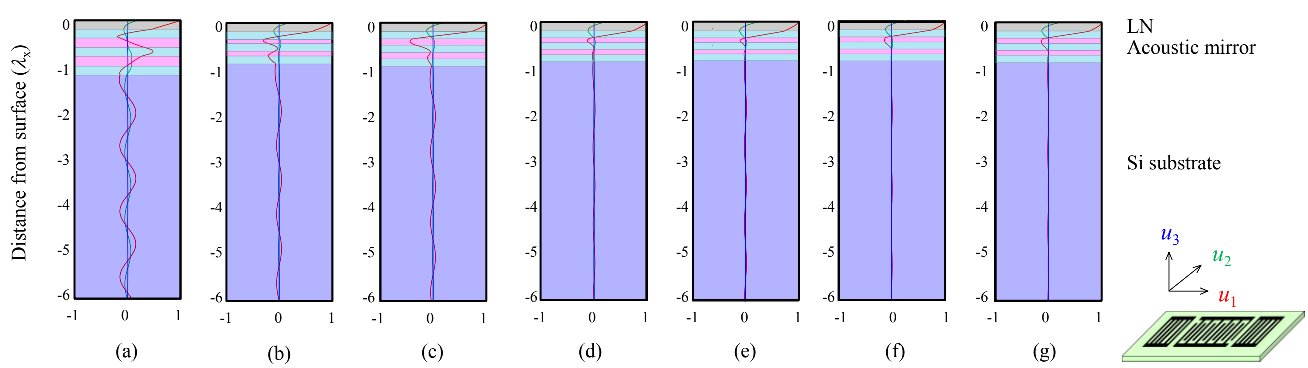

Fig. 8. Simulated cross-sectional field distribution of the structures using several configurations of acoustic mirrors; (a) AlN, (b) Ta_2O_5, (c) HfO_2, (d) Ta, (e) Pt, (f) W and (g) Ir for the HAI materials, respectively. X-axis indicates normalized displacement. Red, green and blue lines in each figure show longitudinal component u_1 (parallel to the propagation direction on the LN surface), share horizontal component u_2 (normal to the u_1 component on the LN surface), and vertical component u_3 (normal to the LN surface), respectively.

III. Observational Validation of the Aoustic Mirror Effect

Developing SAW devices, direct observation of the SAW propagation is useful for finding clues to improve the SAW devices as well as computer simulation and trial production. Thus, several techniques have been reported for diagnosis of acoustic waves by laser probe systems based on knife-edge methods [35-39], the Michelson interferometer [40-45], polarization-detection methods [46-48] and the Sagnac interferometer [49-52]. Most of them are reported on the observation of the SH and Rayleigh SAWs because the both SAWs have been widely used for RF SAW devices in mobile phones. To the best of authors' knowledge, there is only one report on visualizing the LLSAW on a Y cut Z LN substrate with the Michelson interferometer [44].

The authors introduced observation of the LLSAW propagating on the X cut LN thin plate on the acoustic mirror bonded on the silicon substrate [53]. For the observation, the authors used a laser probe system based on the Sagnac interferometer as illustrated in Fig. 9.

As for the measurement principle in a nutshell, an incident laser beam launched from He-Ne laser (wavelength: 632.8 nm) is beam-shaped and divided into two beams in the Sagnac loop. A different optical path between the two beams in the Sagnac loop results in a difference of the arrival time to the surface of a device under test (DUT). Optical phase difference between the two beams occurs, provided that the surface of the DUT is vibrating. The optical signals are detected by a photo detector, and then processed by a detection electronics system [50] undescribed in Fig. 9. It is possible to simultaneously obtain both the amplitude and phase information of the surface vibration. The system proved observation of high frequency surface vibration on DUTs in minutes order.

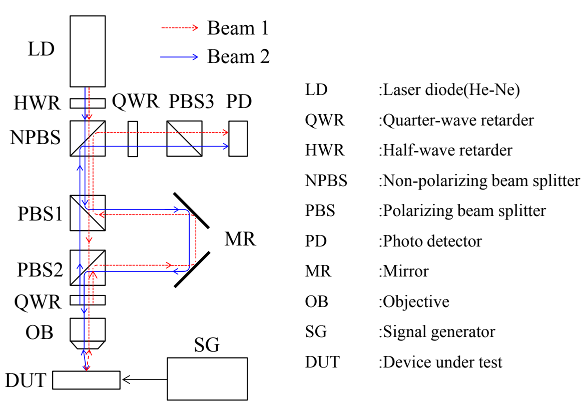

Fig. 9. Configuration of the laser probe system.

Fig. 10 illustrates schematic two test pieces for the observation. Both the sample A and sample B are composed of Al electrodes, the X-cut 40°Y LN thin plate, the acoustic mirror stacked SiO_2 films for the LAI and Pt films for the HAI alternately bonded on the silicon substrate. The Al-IDT of 150 nm thickness are fabricated on the surface of the thin LN plate,

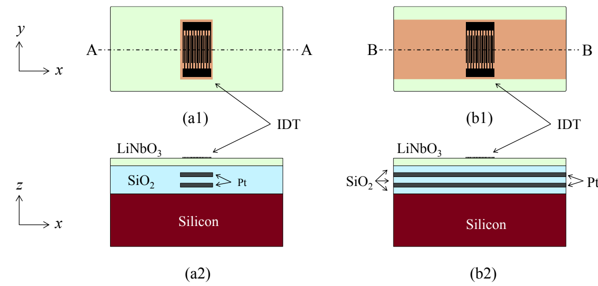

Fig. 10. Schematic top (a1, b1) and cross-sectional (a2, b2) views of the test samples. The sample A (a1, a2) has only the acoustic mirror right under the IDT, and the sample B (b1, b2) has the acoustic mirror underneath not only the IDT but also both sides of it.

and their periodicity, the number of finger pairs and their aperture length are set to 3 μm, 10 pairs and 30 μm, respectively. No grating reflectors are placed at both sides of the IDT. The acoustic mirror is deployed between the LN thin plate and the silicon substrate, and the structural difference between the two samples is that the sample A has only the acoustic mirror right under the IDT hence no acoustic mirror outside of the IDT region, while the sample B has the acoustic mirror underneath the IDT and also both sides of it. The thicknesses of the LN plate, SiO_2 films, and Pt films are 600 nm, 420 nm, and 270 nm, respectively.

A driving RF incident power was 10 dBm, and its frequency was set to 2 GHz, which corresponds to a phase velocity of 6,000 m/s. Scanning steps along x and y of a sample stage were both 400 nm.

Fig. 11 summarizes the comparison results between the sample A and B. According to the observational images of the sample A shown in (a2) of Fig. 11, the vibration pattern is clearly visible only near the IDT region and it decays rapidly as the traveling waves leave from the IDT. In contrast, the vibration pattern shown in (b2) of Fig. 11 does not decay significantly, it is clearly observable even for regions far from the IDT. These observational results demonstrate that the proposed LLSAW structure provides small propagation loss owing to good confinement of acoustic wave energy near the surface of the LN plate in the sample B. The LLSAW, by contrast, in the sample A shows relatively large propagation loss because of lack of the acoustic mirror outside of the IDT region, in other words, non-negligible acoustic energy is leaked away to the silicon substrate.

Figs. 11 (a3) and (b3) show the simulated cross-sectional field distributions, and the simulation agrees well with the observation results. It is clearly seen that acoustic wave energy is trapped in the vicinity of the LN plate owing to the acoustic mirror in the sample B, whereas the acoustic wave energy radiates into the bottom of silicon substrate from the outer edges of the acoustic mirror in the sample A.

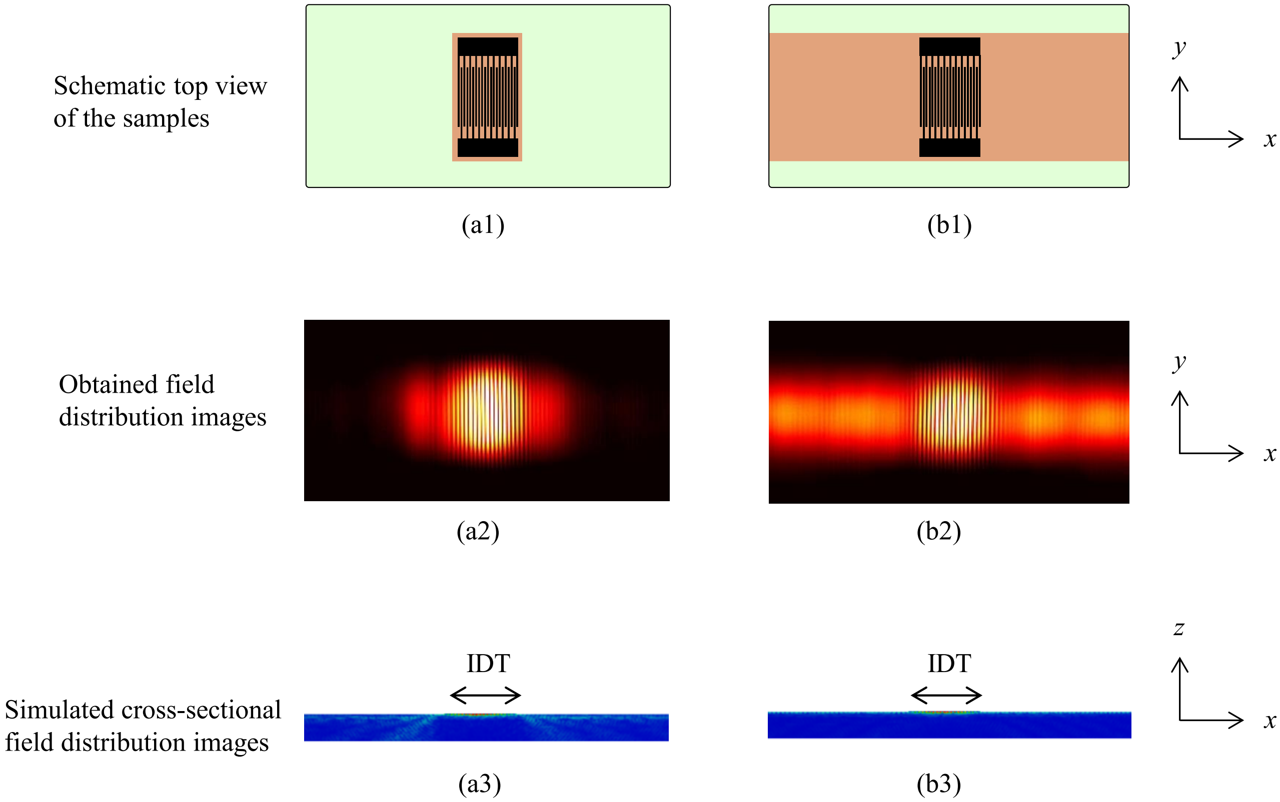

Fig. 11. Comparison results of the observation. (a1) and (b1) show the schematic top views of the sample A and B. (a2) and (b2) are the measured field distribution images of the sample A and B. (a3) and (b3) depict simulated cross-sectional field distribution of the sample A and B by a 3D-FEM.

IV. Experimental Results and Discussion

Fig. 12 shows characteristics of the 3.5 GHz 1-port LLSAW resonator presented in [54]. The structural design parameters are shown in Table III. An equivalent circuit for a piezoelectric resonator called the *modified Butterworth-Van Dyke* (mBVD) model [55, 56] was introduced to characterize the SAW resonator. As seen in Fig 12, there is a good agreement between measured characteristics and fitted ones.

The measured impedance ratio and fractional bandwidth were 71 dB and 9.5%, respectively. The bandwidth is about three times larger than those of conventional 42LT and TC-SAW.

The resonance frequency was 3.55 GHz, it corresponds to a phase velocity of 6,035 m/s. The obtained phase velocity is approximately 1.5 times higher than those of the conventional ones. Q_{max} estimated by Bode-Q [57] was 665.

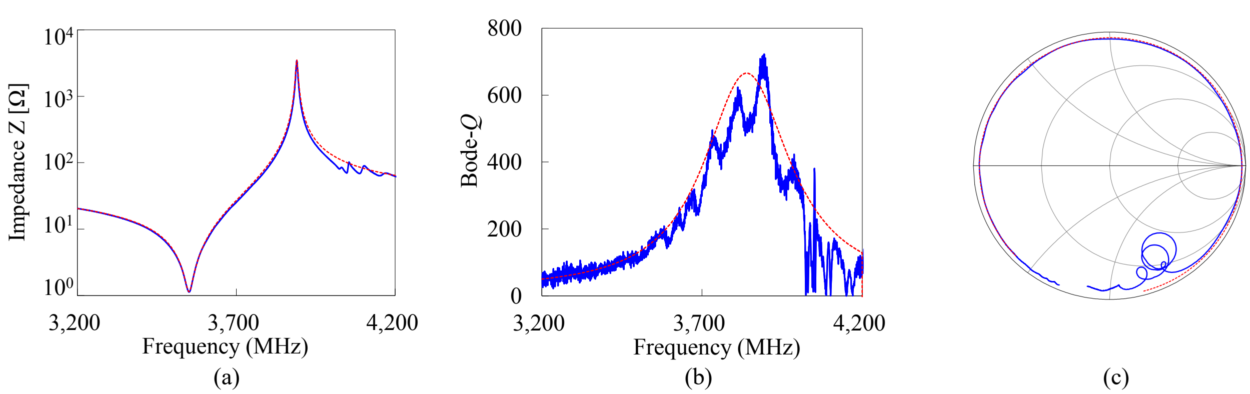

Fig. 12. Measured and fitted characteristics of a 3.5 GHz LLSAW resonator for (a) impedance curve, (b) Bode-Q and (c) Smith chart. Blue solid lines and red dotted lines present experimental results and fitted results by mBVD model, respectively.

TABLE III. 1-PORT SAW STRUCTURAL PARAMETERS FOR EXPERIMENT.

Piezoelectric crystal	Material	$LiNbO_3$
	Euler angle	(90°,90°,40°)
	Thickness	0.34 μm
Electrodes	Wavelength	1.7 μm
	Material	Al
	Thickness	0.08 μm
	Number of pairs	100
	Metallization ratio	0.5
	Aperture	25.5 μm
	Number of reflector	20
Acoustic mirror	Configuration	$SiO_2/Pt/SiO_2/Pt/SiO_2$
	SiO_2 thickness	0.238 μm
	Pt thickness	0.153 μm
Handle substrate	Material	Silicon

Next, a 5 GHz 1-port SAW resonator was demonstrated for comparing to the 3.5 GHz 1-port SAW resonator. Fabrication of the 5 GHz resonator was carried out for the wavelength λ = 1.2 μm, changed from 1.7 μm for the 3.5 GHz resonator. All the structural parameters of the resonator were shrunk with the change of λ. Measured and fitted characteristics of the 5 GHz resonator are shown in Fig. 13. Although an impedance at the resonance frequency slightly increases due to increase to the ohmic resistance of shrunk IDTs. Interestingly, the overall performance does not obviously degrade even with the frequency increase.

V. PERFORMANCE COMPARISON

Lastly, let us discuss the applicability of the proposed LLSAW structure in the super high frequency (SHF) range by comparing with the I.H.P. SAW and another ultra-high velocity plate wave device.

A. Comparison with the I.H.P. SAW

Since the propagation loss of the I.H.P. SAW is extremely small, it may make it possible to realize much higher frequency range such as over the 3 GHz range that was considered to be impractical for the SAW devices. The authors fabricated and evaluated a 3.5 GHz I.H.P. SAW resonator, and compared to the 1.9 GHz I.H.P. SAW resonator performance [17]. Fig. 14 shows the comparison results between the 1.9 GHz and 3.5 GHz I.H.P. SAW resonators. Attained Q_{max} of the 3.5 GHz I.H.P. SAW resonator was 1,740 whereas that of 1.9 GHz one was 4,200 because of the frequency difference.

The Q_{max} of the 3.5 GHz I.H.P. SAW shown in Fig. 14 was approximately 3 times larger than that of the 3.5 GHz LLSAW, however, considering their k^2 difference, the latter k^2 is about 3 times larger, it is difficult to say which is better in a word. Suitable structure should be chosen according to desired filter specifications.

The fabricated 3.5 GHz I.H.P. SAW resonator of the wavelength λ was 1.1 μm, namely line and gap widths of the IDT patterns were 0.275 μm. The patterns are manufacturable by KrF lithography systems, which are currently used in the mass production. However, much finer pattern such as less λ of 0.8 μm for 5 GHz range I.H.P. SAWs would requires Herculean efforts.

In contrast, the 5 GHz LLSAW resonator is realizable when λ is set to 1.2 μm without fetal deterioration characteristics, as compared between Figs. 12 and 13. In addition, the λ of 1.2 μm for the 5 GHz LLSAW resonator is even larger than that of the 3.5 GHz I.H.P. SAW due to the high velocity. It means that SAW devices can be practical even in the 5 GHz range.

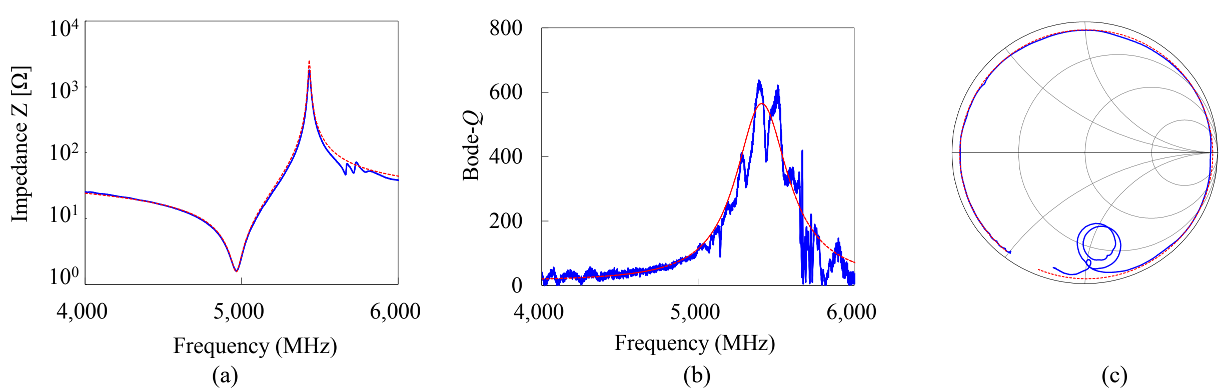

Fig. 13. Measured and fitted characteristics of a 5 GHz LLSAW resonator for (a) impedance curve, (b) Bode-Q and (c) Smith chart. Blue solid lines and red dotted lines present experimental results and fitted results by mBVD model, respectively.

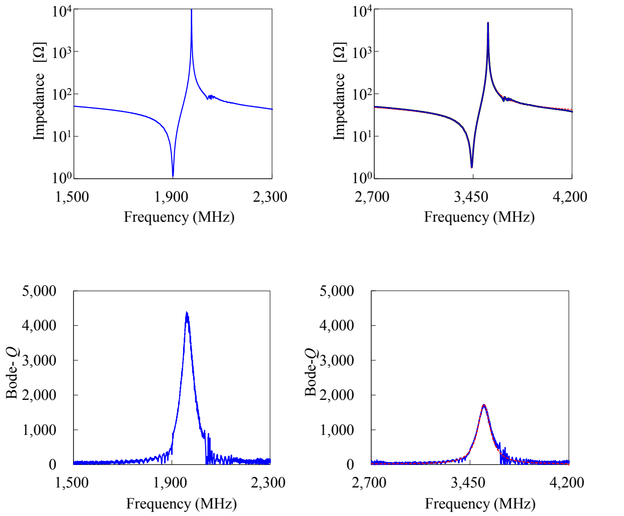

Fig. 14. Comparison between 1.9 GHz and 3.5 GHz I.H.P. SAW resonators for (a1) and (b1) impedance curves, (a2) and (b2) Bode-*Q*. Blue solid lines present experimental results, red dotted lines present fitted results by mBVD model (Fitted curves are drawn only the 3.5 GHz resonator).

B. *Comparison with an A_1 mode Lamb wave device*

Here, let us compare with a much higher SAW-like acoustic wave device. Kadota and Ogami reported a 5.4 GHz A_1 mode Lamb wave resonator using a thin Z cut LN crystal plate [58]. The A_1 mode is a first-order asymmetrical mode whose phase velocity is much higher than several fundamental plate modes when the thickness of the LN is very thin as shown in Fig. 15.

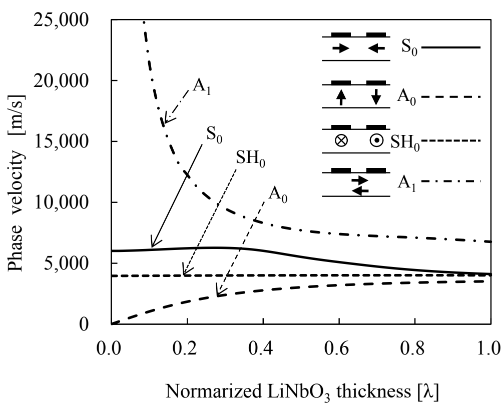

Fig. 15. Calculated several plate waves properties in the thin LN.

Owing to the high phase velocity of around 13,000 m/s, the 5.4 GHz Lamb wave resonator in the thin LN crystal plate was realized even though relatively large wavelength λ of 2.43 μm was set [58].

Comparing with the phase velocities between the proposed LLSAW and the A_1 mode Lamb wave, the latter is 2.2 times higher than former. This clearly indicates that resonators in 10 GHz ranges are realizable with the KrF lithography.

However, the A_1 mode Lamb wave devices have several challenges for practical and stable use in mobile phones. For one thing, precise and accurate LN thickness control is essential because the resonance frequency and k^2 are much more sensitive to the LN thickness in this structure than the LLSAW structure. For another thing, it requires extreme cares for handling because they are potentially fragile. Furthermore, it may be inevitable to apply temperature compensation technique in some way to the A_1 mode Lamb wave devices because the TCF of the original LN plate is not good; around -100 ~ -80 ppm/K. Accumulating SiO_2 films on the IDT as the TC-SAW may give rise to further difficulties such as performance deterioration and frequency control because of its high sensitivity of the thickness.

It should be noted that the proposed structure using the acoustic mirror can be applied to not only the LLSAW (in other word, S_0 mode in the piezoelectric thin plate) but also the other modes including the A_1 mode. Fig. 16 shows an example of simulated impedance curve of the A_1 mode solidly mounted resonator using the acoustic mirror as shown in Fig. 4.

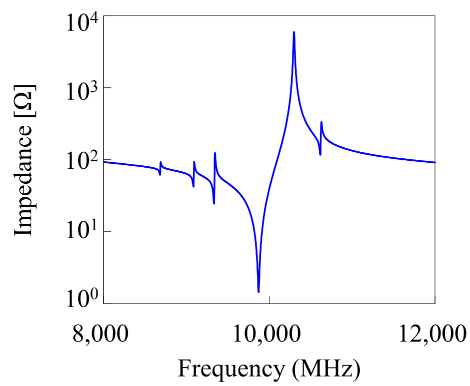

Fig. 16. An example of simulated A_1 mode solidly mounted resonator performance.

For the simulation, the thickness of the Z cut LN and wavelength of the IDT are set to 240 nm and 1.2 μm respectively that their values are the same as the 5 GHz LLSAW resonator shown in Fig. 13. A single-mode resonance is seen at 9.87 GHz, and three spurious responses at frequencies lower than the main response are caused by mirror modes [59], another spurious response resulted from an SH_1 mode appears at above the anti-resonance frequency of the main resonance. The simulation result indicates that a 10 GHz range high frequency resonator is achievable by using a manageable wavelength of 1.2 μm, provided that optimized combination of high-order Lamb wave modes and a structure configuration including the acoustic mirror

VI. Conclusion

This paper discussed an LLSAW device comprising a thin LN crystal plate and an acoustic mirror bonded on a silicon substrate which can offer a high velocity and wideband characteristics.

It was theoretically and experimentally shown how the acoustic mirror is useful for the LLSAW, and it is expected to be promising for sub 6 GHz range filters in the upcoming next generation wireless access technology through comparing with the I.H.P. SAW and a high velocity A_1 Lamb wave resonator.

It was also presented that a 10 GHz range, durable and manageable IDT pitch SAW device was possible by using the acoustic mirror.

AKNOWLEDGMENT

The authors would like to acknowledge engineers of Murata Manufacturing Co., Ltd. for their valuable discussions and support.

REFERENCES

[1] Cisco Visual Networking Index: Global Mobile Data Traffic Forecast Update, 2017–2022, 2019, p.5.

[2] https://www.3gpp.org/

[3] K. Sezawa, "Dispersion of elastic waves propagated on the surface of stratified bodies and on curved surfaces," *Bull. Earthquake Res. Inst*., 3, 1, 1927.

[4] T. Kasanami, H. Ieki, and J. Koike, "1.8 GHz SAW filter," in *Proc. 6th Meet. Ferroelectr. Mater. and Their Appl., Jpn. J. Appl. Phys*., 26, Suppl., 1987, pp. 210-212.

[5] J. Koike, K. Shimoe, and H. Ieki, "1.5 GHz low-loss surface acoustic wave filter using ZnO/Sapphire substrate," *Jpn. J. Appl. Phys*., 32, 5B, 1993, pp. 2337-2340.

[6] S. Fujii, Y. Seki, K. Yoshida, H. Nakahata, K. Higaki, H. Kitabayashi, and S. Shikata, "Diamond wafer for SAW application," in *Proc. IEEE Ultrason. Symp*., 1997, pp. 183-186.

[7] S. Shikata, H. Nakahata, S. Fujii, A. Hachigo, H. Kitabayashi, K. Itakura, T. Uemura, H. Toyoda, and N. Fujimori, "High frequency SAW devices using SiO_2/ZnO/diamond," in *Proc. Int. Symp. Acoust. Wave Devices for Future Mobile Comm. Syst*., 2001, pp. 227-231.

[8] T. Omori, A. Kobayashi, Y. Takagi, K. Hashimoto, and M. Yamaguchi, "Fabrication of SHF range SAW devices on AlN/diamond substrate," in *Proc. IEEE Ultrason. Symp*., 2008, pp. 196-200.

[9] S. Fujii and C. Jian, "High-frequency SAW filters based on diamond films," *IEEE Trans. Ultrason., Ferroelectr*., *Freq. Contr*., **59**, 12, 2012, pp. 2758-2764.

[10] K. Hashimoto, S. Sato, A. Teshigahara, T. Nakamura, and K. Kano, "High-performance surface acoustic wave resonators in the 1 to 3 GHz range using a ScAlN/6H-SiC structure," *IEEE Trans. Ultrason., Ferroelectr*., *Freq. Contr*., **60**, 3, 2013, pp. 637-642.

[11] T. Sato and H. Abe, "Propagation properties of longitudinal leaky surface waves on lithium tetraborate," *IEEE Trans. Ultrason., Ferroelectr*., *Freq. Contr*., **45**, 1, 1998, pp. 136-151.

[12] S. Tonami, A. Nishikata, and Y. Shimizu, "Characteristics of leaky surface acoustic waves propagating on $LiNbO_3$ and $LiTaO_3$ substrates," *Jpn. J. Appl. Phys*., **34**, 5B, 1995, pp. 2664-2667.

[13] Y. Kobayashi, N. Tanaka, K. Matsui, H. Okano, T. Usuki, and K. Shibata, "1.9-GHz-band surface acoustic wave device using second leaky mode on $LiTaO_3$," *Jpn. J. Appl. Phys*., **35**, 5B, 1996, pp. 2987-2990.

[14] A. Isobe, M. Hikita, and K. Asai, "Propagation characteristics of longitudinal leaky SAW in Al-grating structure," *IEEE Trans. Ultrason., Ferroelectr*., *Freq. Contr*., **46**, 4, 1999, pp. 849-855.

[15] T. Makkonen, V. P. Plessky, W. Steichen, and M. M. Salomaa, "Surface-acoustic-wave devices for the 2.5–5 GHz frequency range based on longitudinal leaky waves," *Appl. Phys. Lett.*, **82**, 2003, pp. 3351–3353.

[16] T. Takai, H. Iwamoto, Y. Takamine, H. Yamazaki, T. Fuyutsume, H. Kyoya, T. Nakao, H. Kando, M. Hiramoto, T. Toi, M. Koshino, and N. Nakajima, "High-performance SAW resonator on new multilayered substrate using $LiTaO_3$ crystal," *IEEE Trans. Ultrason., Ferroelectr., Freq. Contr*., **64**, 9, 2017, pp. 1382-1389.

[17] T. Takai, H. Iwamoto, Y. Takamine, T. Fuyutsume, T. Nakao, M. Hiramoto, T. Toi, and M. Koshino, "High-performance SAW resonator with simplified $LiTaO_3$/SiO_2 double layer structure on Si Substrate," *IEEE Trans. Ultrason., Ferroelectr., Freq. Contr*., **66**, 5, 2019, pp. 1006-1013.

[18] M. Kadota and S. Tanaka, "Simulation of solidity mounted plate wave resonator with wide bandwidth using 0-th shear horizontal mode in $LiNbO_3$ plate," *Jpn. J. Appl. Phys*., **54** (2015) 07HD09.

[19] M. Kadota and S. Tanaka, "Near-zero TCF of HAL SAW resonator with $LiTaO_3$-on-quartz structure," in *Proc. IEEE Freq. Cont. Symp*., 2018, 10.1109/FCS.2018.8597496.

[20] M. Kadota, Y. Ishii, T. Shimatsu, M Uomoto, and S. Tanaka, "Suprious-free, near-zero-TCF hetero acoustic layer (HAL) SAW resonators using $LiTaO_3$ thin plate on quartz," in *Proc. IEEE Freq. Cont. Symp*., 2018, 10.1109/ULTSYM.2018.8580111.

[21] J. Hayashi, M. Gomi, M. Suzuki, S. Kakio, H. Suzaki, T. Yonai, K. Kishida and J. Mizuno, "High-coupling leaky SAWs on $LiTaO_3$ thin plate bonded to quartz substrate," in *Proc. IEEE Ultrason. Symp*., 2017, 10.1109/ULTSYM.2017.8091675.

[22] N. Naumenko, "Solidly mounted plate mode resonators based on 42°-48°LT cuts: loss mechanisms," in *Proc. IEEE Ultrason. Symp*., 2017, 10.1109/ULTSYM.2017.8092512.

[23] N. Naumenko, "Suppression of propagation losses in TC SAW resonators using thin plates of $LiTaO_3$ bonded to quartz substrates," in *Proc. IEEE Ultrason. Symp*., 2018, 10.1109/ULTSYM.2018.8579813.

[24] S. Inoue and M. Solal, "Spurious free SAW resonators on layered substrate with ultra-high Q, high coupling and small TCF," in *Proc. IEEE Ultrason. Symp*., 2018, 10.1109/ ULTSYM.2018.8579852.

[25] T. Kimura, K. Daimon, T. Ogami, and M. Kadota, "S_0 mode Lamb wave resonators using $LiNbO_3$ thin plate on acoustic multilayer reflector," *Jpn. J. Appl. Phys*., **52**, 2013, pp. 07HD03(1-4).

[26] T. Kimura, Y. Kishimoto, M. Omura, and K. Hashimoto, "3.5 GHz longitudinal leaky surface acoustic wave resonator using a multilayered waveguide structure for high acoustic energy confinement," *Jpn. J. Appl. Phys*., **57**, 2018, pp. 07LD15(1-4).

[27] T. Kimura, M. Omura, Y. Kishimoto, and K. Hashimoto, "Comparative study of acoustic wave devices using thin piezoelectric plates in the 3-5-GHz range," *IEEE Trans. Microw. Theory Tech*., **67**, 3, 2019, pp. 915-921.

[28] K. M. Lakin, K. T. McCarron, and R. E. Rose, "Solidly mounted resonators and filters," in *Proc. IEEE Ultrason. Symp*., 1995, pp. 905-908.

[29] H. Kanbara, H. Kobayashi, and K. Nakamura, "Analysis of piezoelectric thin film resonators with acoustic quarter-wave multilayers," *Jpn. J. Appl. Phys*., **39**, 2000, pp. 3049-3053.

[30] H. Kobayashi, Y. Ishida, K. Ishikawa, A. Doi, and K. Nakamura, "Analysis of piezoelectric thin film resonators with acoustic quarter-wave multilayers," *Jpn. J. Appl. Phys*., **41**, 2002, pp. 3455-3457.

[31] R. Aigner, J. Ellä, H.-J. Timme, L. Elbrecht, W. Nessler, and S. Marksteiner, "Advancement of MEMS into RF-filter applications," in *Proc. IEEE Int. Electron Devices Meet. Dig*., 2002, pp. 897-900.

[32] R. Aigner, J. Kaitila, J. Ellä, L. Elbrecht, W. Nessler, M. Handtmann, T. Herzog, and S. Marksteiner, "Bulk-acoustic-wave filters: performance optimization and volume manufacturing," in *Proc. IEEE Microw. Theory Techn. Symp*., 2003, pp. 2001-2004.

[33] K. Hashimoto (editor), *RF-Bulk Acoustic Wave Filters for Communications*, Artech House 2009, pp. 27-29.

[34] M. J. S. Lowe, "Matrix techniques for modeling ultrasonic waves in multilayered media," *IEEE Trans. Ultrason., Ferroelectr., Freq. Contr*., **42**, 4, 1995, pp. 525-542.

[35] G. I. Stegeman, "Optical probing of surface waves and surface wave devices," *IEEE Trans. Sonics and Ultrason*., **SU-23**, 3, 1976, pp. 33-36.

[36] H. Engan, "Phase sensitive laser probe for high-frequency surface acoustic wave measurements," *IEEE Trans. Sonics and Ultrason*., **SU-23**, 5, 1978, pp. 372-377.

[37] S. Jen and C.S. Hartmann, "Recent advances in SAW laser probe," in *Proc. IEEE Ultrason. Symp*., 1996, pp.33-36.

[38] H. Kamizuma, T. Omori, K. Hashimoto, and M. Yamaguchi, "Development of fast-scanning laser probe system based on Knife-edge method for diagnosis of surface acoustic wave devices," *IEEE Trans. Ultrason., Ferroelectr., Freq. Contr.*, **52** , 2006, pp. 1186-1191.

[39] H. Kamizuma, L. Y. Yang, T. Omori, K. Hashimoto, and M. Yamaguchi, "High-speed laser probing system for surface acoustic wave devices based on Knife-edge method," *Jpn. J. Appl. Phys.*, **44**, 6B, 2005, pp. 4535-4538.

[40] J. Knuuttila, P. T. Tikka, T. Thorvaldsson, V. P. Plessky, and M. M. Salomaa, "Recent advances in laser-interferometric investigations of SAW devices," in *Proc. IEEE Ultrason. Symp.*, 1997, pp. 161-164.

[41] J. Knuuttila, P. T. Tikka, T. Thorvaldsson, K. Hashimoto, and M. M. Salomaa, "High resolution laser-interferometric probing of SAW devices," in *Proc. IEEE Ultrason. Symp.*, 1998, pp. 235-238.

[42] H. Yatsuda, S. Kamiseki, and T. Chiba, "Calculation and optical measurement of SAW diffraction pattern of slanted finger SAW filters on YZ $LiNbO_3$ and 128YX $LiNbO_3$," in *Proc IEEE Ultrason. Symp.*, 2001, pp. 13-17.

[43] K. Kokkonen, J. V. Knuuttila, V. P. Plessky, and M. M. Salomaa, "Phase-sensitive absolute-amplitude measurements of surface waves using heterodyne interferometry," in *Proc. IEEE Ultrason. Symp.*, 2003, pp. 1145-1148.

[44] O. Holmgren, J. V. Knuuttila, T. Makkonen, K. Kokkonen, V. P. Plessky, W. Steichen, M. Solal, and M. M. Salomaa, "Imaging surface-acoustic fields in a longitudinal leaky wave resonator," *Appl. Phys. Lett.*, 2005, **86**, 024101.

[45] O. Holmgren, T. Makkonen, J. V. Knuuttila, V. P. Plessky, and W. Steichen, "Laser-interferometric analysis of Rayleigh wave radiation from a LLSAW resonator," in *Proc. IEEE Ultrason. Symp.*, 2007, pp. 1905-1908.

[46] A. Miyamoto, S. Wakana, and A. Ito, "Novel optical observation technique for shear horizontal wave in SAW resonators on 42◦YX-cut lithium tantalate," in *Proc. IEEE Ultrason. Symp.*, 2002, pp. 89–92.

[47] S. Wakana, A. Miyamoto, and A. Ito, "Backside observation technique for SAW distribution under electrodes," in *Proc. IEEE Ultrason. Symp.*, 2003, pp. 1714-1717.

[48] A. Miyamoto, S. Matsuda, S. Wakana, and A. Ito, "Optical observation technique for SH-type surface acoustic wave," *Trans. Inst. Electron. Commun. Eng., Japan*, **86**, 12, 2003, pp.1295-1301.

[49] T. Tachizaki, T. Murota, O. Matsuda, Y. Sugawara, D. H. Hurley, and O. B. Wright, "Scanning ultrafast Sagnac interferometry for imaging surface wave propagation," *Review of Sci. Instrum.*, **77**, 2006, pp. 043713(1-12).

[50] K. Hashimoto, K. Kashiwa, N. Wu, T. Omori, M. Yamaguchi, O. Takano, S. Meguro, and K. Akahane, "A laser probe based on a Sagnac interferometer with fast mechanical scan for RF surface and bulk acoustic wave devices," *IEEE Trans. Ultrason., Ferroelectr., Freq. Contr.*, **58**, 2011, pp. 187-194.

[51] K. Hashimoto and T. Omori, "Phase-sensitive and fast-scanning laser probe system for radio frequency surface/bulk acoustic wave devices," in *Proc. Eur. Freq. and Time Forum*, 2014, pp. 56-59.

[52] T. Omori, T. Suzuki, and K. Hashimoto, "Development of fast scanning SAW/BAW probing system for RF devices and its applications - Implementation of frequency scanning function-," in *Proc. Int. Symp. Acoust. Wave Devices for Future Mobile Comm. Syst.*, 2018.

[53] T. Kimura, H. Kyouya, H. Okunaga, M. Omura, and K. Hashimoto, "Observational and theoretical validation of longitudinal type surface acoustic wave devices," *Jpn. J. Appl. Phys.*, **58**, 2019, pp. SGGC04(1-7).

[54] T. Kimura, Y. Kishimoto, M. Omura, and K. Hashimoto, "3.5 GHz longitudinal leaky surface acoustic wave resonator using a multilayered waveguide structure for high acoustic energy confinement," *Jpn. J. Appl. Phys.*, **57**, 2018, pp. 07LD15(1-4).

[55] The piezoelectric vibrator: Definitions and methods of measurements, IRE Standards on Piezoelectric crystals 57 in *Proc. of the I.R.E.*, 1957, pp. 353-358.

[56] J. Larson, P. Bradley, S. Wartenberg, and R. Ruby, "Modified Butterworth-Van Dyke circuit for FBAR resonators and automated measurement system," in *Proc. IEEE Ultrason. Symp.*, 2000, pp. 863-868.

[57] D. A. Feld, R. Parker, R. Ruby, P. Bradley, and S. Dong, "After 60 years: A new formula for computing quality factor is warranted," in *Proc. IEEE Ultrason. Symp.*, 2008, pp. 431-436.

[58] M. Kadota and T. Ogami "5.4 GHz Lamb wave resonator on $LiNbO_3$ thin crystal plate and its application," *Jpn. J. Appl. Phys.*, **50**, 2011, pp. 07HD11(1-4).

[59] R. Aigner and A. Tajic, "Temperature compensated bulk acoustic wave devices using over-moded acoustic reflector layers," US Patent Application US14/044782, 2013.